BLIND IMAGE DEBLURRING USING JUMP REGRESSION ANALYSIS

Peihua Qiu and Yicheng Kang

Department of Biostatistics, University of Florida

Abstract: Observed images are often blurred. Blind image deblurring (BID) is for estimating a true image from its observed but blurred version, when the blurring mechanism described by a point spread function (psf) cannot be completely specified beforehand. This is a challenging "ill-posed" problem, because (i) theoretically speaking, the true image cannot be uniquely determined by the observed image when the psf is unknown, and (ii) practically, besides blur, observed images often contain noise that would bring numerical instability to the image deblurring problem. In the literature, early image deblurring methods are developed under the assumption that the psf is known. More recent methods try to avoid this restrictive assumption, by assuming that either the psf follows a parametric form with some unknown parameters, or the true image has certain special structures. In this paper, we propose a BID methodology, without imposing restrictive assumptions on the psf or the true image. It even allows the psf to change over location. Our method makes use of the hierarchical nature of blurring that the image structure is altered most significantly around step edges, less significantly around roof/valley edges, and least significantly at places where the true image intensity function is straight. So, it pays special attention to regions around step and roof/valley edges when deblurring. Theoretical justifications and numerical studies show that it works well in applications.

Key words and phrases: Deconvolution, denoising, edges, jump-preserving surface estimation, local smoothing, nonparametric regression, principal components.

1 Introduction

Observed images generated by image acquisition devices are usually not exactly the same as the true images, but are degraded versions of their true images (e.g., Gonzalez and Woods 1992, Qiu 2005). Degradations can occur in the entire image acquisition process, and there are many different sources of degradation.

For instance, in aerial reconnaissance, astronomy, and remote sensing, images are often degraded by atmospheric turbulence, aberrations of the optical system, or relative motion between the camera and the object. Among different degradations, *point degradation* (or, noise) and *spatial degradation* (or, blurring) are the most common in practice. Other types of degradations involve chromatic or temporal effects. See Bates and McDonnell (1986) for a detailed discussion about formation and description of various degradations.

In the literature, a commonly used model for describing the relationship between a true image f and its observed but degraded version Z is as follows.

$$Z(x,y) = H\{f\}(x,y) + \varepsilon(x,y), \quad \text{for } (x,y) \in \Omega, \tag{1}$$

where $H\{f\}(x,y) = \int\int_{R^2} h(u,v;x,y)f(x-u,y-v)\,dudv$ denotes the convolution between a 2-D *point spread function (psf)* h and the true image intensity function f, $\varepsilon(x,y)$ is the pointwise noise at (x,y), and Ω is the design space of the image. In model (1), it is assumed that f is degraded spatially by h and pointwise by ε, the spatial blur is linear, and the pointwise noise is additive. In most references, people further assume that h, which describes the spatial blurring mechanism, is location invariant. That is, $h(u,v;x,y)$ does not depend on (x,y).

Image deblurring is for estimating f from Z. This problem is "ill-posed" for the following reasons. First, even in cases when no noise is contained in Z, there could be multiple sets of h and f that correspond to the same Z, when h is unspecified beforehand. Second, the inverse problem to estimate f from Z is often numerically unstable, caused mainly by noise. For instance, in cases when h is location invariant and known, from (1), we have

$$\mathcal{F}\{Z\}(u,v) = \mathcal{F}\{h\}(u,v)\mathcal{F}\{f\}(u,v) + \mathcal{F}\{\varepsilon\}(u,v), \quad \text{for } (u,v) \in R^2,$$

where $\mathcal{F}\{f\}$ denotes the Fourier transformation of f. Then, an intuitively reasonable estimator of f can be defined by the inverse Fourier transformation of $\mathcal{F}\{Z\}(u,v)/\mathcal{F}\{h\}(u,v)$. However, when u^2+v^2 gets larger, $\mathcal{F}\{h\}(u,v)$ converges to zero fast because h is usually a smooth function, but $\mathcal{F}\{Z\}(u,v)$ converges to zero much slower because of the high-frequency noise in Z. Therefore, such an estimator would be numerically unstable.

In the literature, early image deblurring procedures are under the assumption that h is completely specified. In such cases, a major challenge is to overcome

the numerical difficulty mentioned above. To this end, many proposals have been suggested, including the inverse filtering, Wiener filtering, Lucy-Richardson algorithm, maximum *a posteriori* (MAP) procedure, total variation image deblurring, and so forth (e.g., Biggs and Andrews 1997, Figueiredo and Nowak 2003, Gonzalez and Woods 1992, Skilling 1989, Oliveira, Bioucas-Dias, and Figueiredo 2009). In practice, however, it is often difficult to specify h. Image deblurring when h is unspecified is referred to as the *blind image deblurring (BID)* problem, which is challenging due to its "ill-posed" nature described above. There are some existing procedures to handle the BID problem. Some of them assume that h follows a parametric model with one or more unknown parameters, and estimate the parameters together with the true image f (e.g., Carasso 2001, Hall and Qiu 2007a, Joshi and Chaudhuri 2005, Katsaggelos and Lay 1990). Some others assume that f has one or more regions with certain known edge structures (e.g., Hall and Qiu 2007b, Kundur and Hatzinakos 1996, Qiu 2008). Several authors formulate the BID problem as a regularization problem with regularization measures on both h and f (e.g., Chan and Wong 1998, Pruessner and O'Leary 2003, Rudin, Osher and Fatemi 1992, You and Kaveh 1996). Some others develop BID methods under the Bayesian framework (e.g., Fergus, Singh, Hertzmann, Roweis, and Freeman 2006, Likas and Galatsanos 2004). For overviews on this topic, see Kundur and Hatzinakos (1996) and Levin, Weiss, Durand, and Freeman (2011).

In practice, the model assumptions required by the existing methods described above are often invalid, or difficult to check. For instance, the blur in a satellite image is usually caused by wind, turbulence, relative motion between the satellite and the earth, imperfection of the camera lens, and so forth. The psf h in such cases is difficult to specify by a parametric model. It may not be location invariant either. As demonstrated by several authors (e.g., Carasso 2001, Hall and Qiu 2007b), image deblurring results are sensitive to the specification of h. Therefore, the ill-posed BID problem is still mostly open.

In this paper, we propose a novel approach to the BID problem without imposing restrictive assumptions on either h or f. It even allows h to change over location. We notice that image blurring has the following hierarchical nature. Namely, *it alters the image structure most significantly at step edges (i.e., places where f has jumps), less significantly at roof/valley edges (i.e., places where the*

first-order derivatives of f have jumps), and least significantly at places where *f is straight.* Therefore, we pay special attention to regions around jumps in f and in its derivatives of different orders. In practice, jumps in the second or higher order derivatives of f is hardly visible. So, only step and roof/valley edges are specially treated in this paper, although jumps in the second or higher order derivatives of f can be treated similarly. The major statistical tool used here is the jump regression analysis (JRA) (cf., Qiu 2005). Under that framework, model (1) is regarded as a 2-dimensional (2-D) regression model, f is a jump regression surface, and various edges correspond to jumps in f and in its derivatives of different orders. Local smoothing procedures are proposed under that framework for estimating f by removing both pointwise noise and spatial blur. Theoretical justifications and numerical studies show that it works well in applications.

The remaining part of the article is organized as follows. In the next section, our proposed methodology is described in detail. Some of its statistical properties are presented in Section 3. Its numerical performance is investigated in Section 4. Discussions about future research are presented in Section 5. Technical details and some numerical results are provided in a supplementary file.

2   Methodology

2.1   Step and Roof/Valley Edge Detection

In the literature, existing edge detection procedures focus mainly on cases when the observed image contains pointwise noise but it has no spatial blur involved (e.g., Canny 1986, Chu, Siao, Wang and Deng 2011, Garlipp and Müller 2007, Sun and Qiu 2007). Here, we try to take into account the possible blurring in the observed data when detecting edges. For simplicity, let us assume that the design space is $\Omega = [0,1] \times [0,1]$, and $\{(x_i, y_j)\}$ are equally spaced in Ω, i.e., $(x_i, y_j) = (i/n, j/n)$, for $i, \ j = 1, \ldots, n$. Observations $\{(x_i, y_j, Z_{ij}), i, \ j = 1, 2, \ldots, n\}$ are assumed to be from model (1). Namely,

$$Z_{ij} = H\{f\}(x_i, y_j) + \varepsilon_{ij}, \quad \text{for } i, \ j = 1, 2, \ldots, n, \tag{2}$$

where ε_{ij} are i.i.d. errors with mean 0 and unknown variance σ^2. For a given point $(x, y) \in [k_1/n, 1 - k_1/n] \times [k_1/n, 1 - k_1/n]$, where the positive integer $k_1 < n/2$

is a bandwidth, we consider its circular neighborhood

$$O'_n(x,y) = \left\{ (u,v) : (u,v) \in \Omega \text{ and } \sqrt{(u-x)^2 + (v-y)^2} \leq k_1/n \right\}.$$

In this neighborhood, let us consider the following local linear kernel (LLK) smoothing procedure:

$$\min_{a,b,c} \sum_{i^2+j^2 \leq k_1^2} \left[Z\left(x+i/n, y+j/n\right) - \left(a + b\frac{i}{n} + c\frac{j}{n}\right) \right]^2 K^*\left(\frac{i}{k_1}, \frac{j}{k_1}\right), \quad (3)$$

where K^* is a circularly symmetric bivariate density kernel function defined on the unit disk centered at the origin. Let the solution to $\{a, b, c\}$ of the problem (3) be denoted as $\{\widehat{a}(x,y), \widehat{b}(x,y), \widehat{c}(x,y)\}$. Then, $(\widehat{b}(x,y), \widehat{c}(x,y))$ is an estimator of the gradient of the true regression surface f at (x,y). Now, we divide $O'_n(x,y)$ into two halves, denoted as $U'_n(x,y)$ and $V'_n(x,y)$, along the direction perpendicular to $(\widehat{b}(x,y), \widehat{c}(x,y))$. The change in the values of f from $V'_n(x,y)$ to $U'_n(x,y)$ should be relatively large if (x,y) is on a step edge segment. Also, in cases when spatial blur is present, design points in $O'_n(x,y)$ closer to the step edge segment would have more blurring involved. By combining these two facts, we define our step edge detection criterion by

$$\mathrm{M}_n^{(1)}(x,y) = \frac{|\widehat{a}_+(x,y) - \widehat{a}_-(x,y)|}{\sqrt{\frac{\sum_{(x_i,y_j) \in U'_n(x,y)} b_{ij}(x,y)^2}{\left[\sum_{(x_i,y_j) \in U'_n(x,y)} b_{ij}(x,y)\right]^2} + \frac{\sum_{(x_i,y_j) \in V'_n(x,y)} b'_{ij}(x,y)^2}{\left[\sum_{(x_i,y_j) \in V'_n(x,y)} b'_{ij}(x,y)\right]^2}}},$$

where $\widehat{a}_+(x,y)$ and $\widehat{a}_-(x,y)$ are respectively the solutions to a of the following local weighted least square problems:

$$\min_{a,b,c} \sum_{U'_n(x,y)} \left[Z\left(x+\tfrac{i}{n}, y+\tfrac{j}{n}\right) - \left(a + b\tfrac{i}{n} + c\tfrac{j}{n}\right) \right]^2 K^*\left(\tfrac{i}{k_1}, \tfrac{j}{k_1}\right) L^*\left(\tfrac{d'_{ij}}{k_1/n}\right), \quad (4)$$

$$\min_{a,b,c} \sum_{V'_n(x,y)} \left[Z\left(x+\tfrac{i}{n}, y+\tfrac{j}{n}\right) - \left(a + b\tfrac{i}{n} + c\tfrac{j}{n}\right) \right]^2 K^*\left(\tfrac{i}{k_1}, \tfrac{j}{k_1}\right) L^*\left(\tfrac{d'_{ij}}{k_1/n}\right), \quad (5)$$

$$b_{ij}(x,y) = \left[B_1(x,y) + B_2(x,y)\tfrac{i}{n} + B_3(x,y)\tfrac{j}{n} \right] K^*\left(\tfrac{i}{k_1}, \tfrac{j}{k_1}\right) L^*\left(\tfrac{d'_{ij}}{k_1/n}\right),$$

$$B_1(x,y) = t_{20}(x,y)t_{02}(x,y) - t_{11}(x,y)t_{11}(x,y),$$

$$B_2(x,y) = t_{01}(x,y)t_{11}(x,y) - t_{10}(x,y)t_{02}(x,y),$$

$$B_3(x,y) = t_{10}(x,y)t_{11}(x,y) - t_{01}(x,y)t_{20}(x,y),$$

$$t_{s_1,s_2}(x,y) = \sum_{U'_n(x,y)} \left(\tfrac{i}{n}\right)^{s_1} \left(\tfrac{j}{n}\right)^{s_2} K^*\left(\tfrac{i}{k_1}, \tfrac{j}{k_1}\right) L^*\left(\tfrac{d'_{ij}}{k_1/n}\right), s_1, s_2 = 0, 1, 2,$$

5

$b'_{ij}(x, y)$ is defined in the same way as $b_{ij}(x, y)$ except that $U'_n(x, y)$ in the definition of $t_{s_1, s_2}(x, y)$ should be replaced by $V'_n(x, y)$, L^* is a univariate increasing density kernel function with support $[0, 1]$, and d'_{ij} is the Euclidean distance from the point (x_i, y_j) to the line dividing $O'_n(x, y)$ into $U'_n(x, y)$ and $V'_n(x, y)$. Clearly, our step edge detection criterion is a standardized difference between the two one-sided local linear kernel estimators $\widehat{a}_+(x, y)$ and $\widehat{a}_-(x, y)$. By using the two kernel functions K^* and L^*, design points farther away from (x, y) or closer to the line dividing $O'_n(x, y)$ into $U'_n(x, y)$ and $V'_n(x, y)$ would receive less weights. Then, the design point (x, y) is flagged as a detected step edge pixel if

$$\mathrm{M}_n^{(1)}(x, y) > u_n \sigma, \tag{6}$$

where u_n is a threshold value. As pointed out by Qiu and Yandell (1997), detected edge pixels by (6) usually contain two types of deceptive ones: those scattered in the whole design space due to randomness and those around true edge curves due to thresholding. They can be deleted reasonably well by the two modification procedures proposed in that paper. In practice, σ is often unknown, and it needs to be estimated from the observed data. To this end, it can be estimated by the residual mean squares of the conventional LLK smoothing procedure. The estimator of σ is denoted as $\widehat{\sigma}$ hereafter.

A related procedure for detecting roof/valley edges is described in the supplementary file.

2.2 Blind image deblurring

As described in Section 1, our proposed BID procedure pays special attention to regions around the detected step and roof/valley edges when deblurring the observed image Z (or, estimating the true image f from Z). To estimate f at a given design point (x, y), let us consider a circular neighborhood

$$O_n(x, y) = \{(u, v) : \sqrt{(u - x)^2 + (v - y)^2} \leq k/n\},$$

where $k < n/2$ is a positive integer that could be different from the bandwidths k_1 or k_2 used in edge detection. Let $\{(w_l, v_l), l = 1, 2, \ldots, m\}$ be detected step edge points in $O_n(x, y)$, $\bar{w}, \bar{v}, \sigma_{ww}$ and σ_{vv} be the sample means and sample variances of $\{w_l, l = 1, 2, \ldots, m\}$ and $\{v_l, l = 1, 2, \ldots, m\}$, σ_{wv} be their sample covariance,

and (W, V) be a vector variable taking values over $\{(w_l, v_l), l = 1, 2, \cdots, m\}$. To estimate the underlying step edge segment in $O_n(x, y)$ from the detected step edge points, we consider using the principal component (PC) line of the points $\{(w_l, v_l), l = 1, 2, \ldots, m\}$, which goes through the center of these points along the direction that they have the biggest dispersion. See Figure 1(a) for a demonstration. The PC line has the expression

$$\sigma_{wv}(W - \bar{w}) + (\lambda_1 - \sigma_{ww})(V - \bar{v}) = 0, \tag{7}$$

where

$$\lambda_1 = \frac{1}{2}\left(\sigma_{ww} + \sigma_{vv} - \sqrt{(\sigma_{ww} - \sigma_{vv})^2 + 4\sigma_{wv}^2}\right)$$

is the smaller eigenvalue of the sample covariance matrix of $\{(w_l, v_l), l = 1, 2, \ldots, m\}$. In cases when no blurring is involved in Z, Qiu (1998) has shown that this PC line provides a good approximation to the underlying step edge segment if the step edge segment has a unique tangent line at (x, y). In Section 3, we will show that this is still true in cases when Z contains spatial blur.
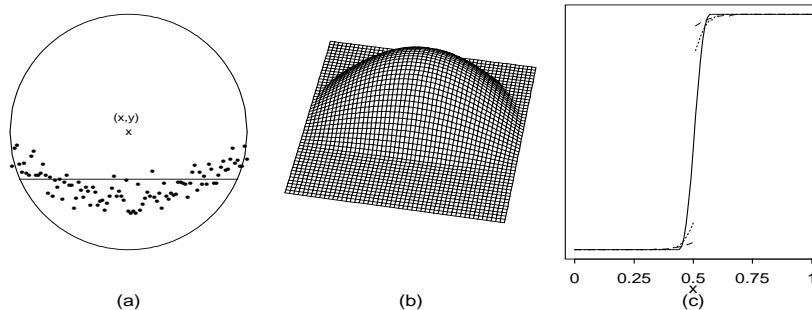

Figure 1: (a): In neighborhood $O_n(x, y)$, the PC line (solid line) goes through the center of the detected step edge points (small dots) along the direction that they have the biggest dispersion. (b): In $O_n(x, y)$, a typical weighting function used in (8) is shown by the surface. (c): A cross section of a blurred image intensity surface around a step edge (solid line) and the deblurred versions by (9) when the bandwidth k/n is relatively small (dotted line) and relatively large (dashed line).

Intuitively, if Z contains no blur, then $f(x, y)$ can be estimated by a weighted average of the observations located on the same side of the PC line as (x, y), as did in the image denoising literature (cf., Qiu 1998). In cases when blurring is present, if a design point in $O_n(x, y)$ is closer to the PC line, then it is more likely that the corresponding observed image intensity has blurring involved, as discussed in

7

Section 2. Thus, it should receive a smaller weight in the weighted average. To address this issue, similar to edge detection, besides a 2-D kernel function used in conventional local smoothing to assign more weights to design points closer to (x, y), a univariate kernel function L is used to assign less weights to design points closer to the PC line. Then, the deblurred image $\widehat{f}(x, y)$ is defined by the solution to a_0 of the following local constant kernel (LCK) smoothing procedure:

$$\min_{a_0 \in R} \sum_{U_n(x,y)} \left\{ Z\left(x + \tfrac{i}{n}, y + \tfrac{j}{n}\right) - a_0 \right\}^2 K\left(\tfrac{i}{k}, \tfrac{j}{k}\right) L\left(\tfrac{d_{ij}}{k/n + d(x,y)}\right), \qquad (8)$$

where K is a circularly symmetric 2-D kernel density function that could be different from the kernel function K^* used in edge detection, L is a univariate increasing density kernel function with support $[0, 1]$ that could also be different from the kernel function L^*, $d(x, y)$ is the Euclidean distance from point (x, y) to the PC line, d_{ij} is the Euclidean distance from point (x_i, y_j) to the PC line, and $U_n(x, y)$ denotes the set of design points in $O_n(x, y)$ that are on the same side of the PC line as (x, y). That is,

$$U_n(x, y) = \begin{cases} \{(x_i, y_j) \in O_n(x, y) : \quad \sigma_{wv}(x_i - \bar{w}) + (\lambda_1 - \sigma_{ww})(y_j - \bar{v}) \geq 0\}, \\ \qquad\qquad \text{if } \sigma_{wv}(x - \bar{w}) + (\lambda_1 - \sigma_{ww})(y - \bar{v}) \geq 0; \\ \{(x_i, y_j) \in O_n(x, y) : \quad \sigma_{wv}(x_i - \bar{w}) + (\lambda_1 - \sigma_{ww})(y_j - \bar{v}) < 0\}, \\ \qquad\qquad \text{otherwise.} \end{cases}$$

By certain routine algebraic manipulations, we have

$$\widehat{f}(x, y) = \frac{\sum_{(x_i, y_j) \in U_n(x,y)} \widetilde{w}_{ij}(x, y) Z_{ij}}{\sum_{(x_i, y_j) \in U_n(x,y)} \widetilde{w}_{ij}(x, y)}, \qquad (9)$$

where $\widetilde{w}_{ij}(x, y) = K(i/k, j/k) L(\frac{d_{ij}}{k/n + d(x,y)})$. By (8) and (9), we actually fit a constant in $O_n(x, y)$, using a weighted average scheme. The weights are controlled by $K(i/k, j/k) L\left(\frac{d_{ij}}{k/n + d(x,y)}\right)$. When K and L are chosen to be the ones used in Section 4 and when the detected step edge points are those shown in Figure 1(a), the weights used in (8) when estimating $f(x, y)$ are demonstrated by the surface shown in Figure 1(b). From the plot, we can see that (i) only those design points that are on the same side of the PC line as (x, y) would receive positive weights, and (ii) a given design point would receive more weight if it is closer to (x, y) and farther away from the PC line. Because of this weighting scheme,

8

the fitted plane in $O_n(x,y)$ is mainly determined by observations whose design points are certain distance away from the PC line. Consequently, $\widehat{f}(x,y)$ would not be affected much by the blurring around the underlying step edge segment in $O_n(x,y)$, especially when the blurring extent $r_n(x,y)$ (see its definition in Section 3) is relatively small, compared to k. In Figure 1(c), a cross section of a blurred image intensity function around a step edge is shown by the solid line. The dotted and dashed lines denote the deblurred image intensity functions by (9) when $k = r_n(x,y)$ and $k = 2r_n(x,y)$, respectively. It can be seen that (i) the BID procedure (9) does have the ability to deblur the image around step edges, and (ii) it would deblur the image better if the ratio r_n/k is smaller. The second conclusion implies that procedure (9) would perform better if the blurring extent is smaller. If the blurring extent is relatively large, then the deblurred image by (9) may still contain certain blur, although the blur is mostly eliminated, because (9) cannot use a very large bandwidth in order to avoid large bias in local smoothing. More theoretical and numerical justifications of (9) are given in the next two sections.

Formula (9) is for image deblurring around the detected step edges. In $O_n(x,y)$, if the number of detected step edge points, denoted as $I'_n(x,y)$, is so small that it is unlikely to have a step edge segment in $O_n(x,y)$ (e.g., $I'_n(x,y) < k$,), then we check to see whether $O_n(x,y)$ would possibly contain a roof/valley edge segment. In the case when the number of detected roof/valley edge points, denoted as $I''_n(x,y)$, is quite large (e.g., $I''_n(x,y) \geq k$) and it is possible to have a roof/valley edge segment in $O_n(x,y)$, $\widehat{f}(x,y)$ can still be defined by (9), except that the detected step edge points $\{(w_l, v_l), l = 1, 2, \ldots, m\}$ should be replaced by the detected roof/valley edge points in its definition. The corresponding estimator $\widehat{f}(x,y)$ should deblur the image well around the detected roof/valley edge points, as explained above about image deblurring around the detected step edge points. In cases when both $I'_n(x,y)$ and $I''_n(x,y)$ are so small that $O_n(x,y)$ is unlikely to contain any step or roof/valley edge segments, we suggest estimating $f(x,y)$ by the conventional LLK estimator, which is the solution to a_0 of the LLK procedure

$$\min_{a_0,a_1,a_2} \sum_{i^2+j^2 \leq k^2} \left[Z\left(x + \tfrac{i}{n}, y + \tfrac{j}{n}\right) - \left(a_0 + a_1\tfrac{i}{n} + a_2\tfrac{j}{n}\right) \right]^2 K\left(\tfrac{i}{k}, \tfrac{j}{k}\right). \qquad (10)$$

9

In such cases, $\widehat{f}(x,y)$ has the expression

$$\widehat{f}(x,y) = \frac{\sum_{i^2+j^2 \le k^2} w_{ij}(x,y) Z_{ij}}{\sum_{i^2+j^2 \le k^2} w_{ij}(x,y)}, \tag{11}$$

where

$$
\begin{aligned}
w_{ij}(x,y) &= \left[A_1(x,y) + A_2(x,y)\frac{i}{n} + A_3(x,y)\frac{j}{n} \right] K\left(\frac{i}{k}, \frac{j}{k}\right), \\
A_1(x,y) &= r_{20}(x,y)r_{02}(x,y) - r_{11}(x,y)r_{11}(x,y), \\
A_2(x,y) &= r_{01}(x,y)r_{11}(x,y) - r_{10}(x,y)r_{02}(x,y), \\
A_3(x,y) &= r_{10}(x,y)r_{11}(x,y) - r_{01}(x,y)r_{20}(x,y), \\
r_{s_1 s_2}(x,y) &= \sum_{i^2+j^2 \le k^2} \left(\frac{i}{n}\right)^{s_1} \left(\frac{j}{n}\right)^{s_2} K\left(\frac{i}{k}, \frac{j}{k}\right), \quad \text{for } s_1, s_2 = 0,1,2.
\end{aligned}
$$

By comparing (11) with (9), it can be seen that, when estimating $f(x,y)$, an LCK estimator is used in (9) in cases when (x,y) is close to a step or roof/valley edge segment, while an LLK estimator is used in (11) in cases when (x,y) is far away from any step or roof/valley edge. That is because the LCK estimator is more robust to spatial blur around edges, as demonstrated by Figure 2, and the LLK estimator is less biased in continuity regions (cf., Qiu 2005, Chapter 2). In practice, a regular image usually contains some regions where no step
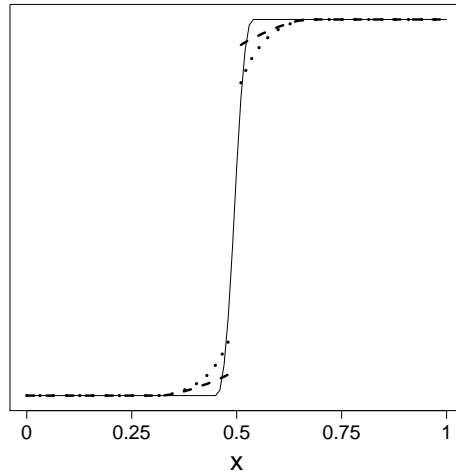

Figure 2: A cross section of a blurred image intensity surface around a step edge (solid line), the deblurred version by (9) with local constant kernel estimation (dashed line), and the deblurred version by (9) with local linear kernel estimation (dotted line).

or roof/valley edge segments are present. So, at a given pixel (x, y), before estimating a PC line from the detected step or roof/valley edge pixels in $O_n(x, y)$, we suggest making a judgment to insure that a step or roof/valley edge segment is possible in $O_n(x, y)$. One major benefit to do so is that the image estimator in (11) would be more efficient than the one in (9) at places without any step or roof/valley edge segments, because of the fact that the former estimator is constructed from all observations in $O_n(x, y)$ while the latter estimator uses only part observations in $O_n(x, y)$. After taking all these considerations into account, our proposed BID procedure is summarized below.

<h3 align="center">Proposed Blind Image Deblurring Procedure</h3>

1. Detect step and roof/valley edge points.

2. At a given point (x, y), if the number of detected step edge points $I_n'(x, y) \geq k$, then estimate $f(x, y)$ by (7)–(9).

3. If $I_n'(x, y) < k$ but $I_n''(x, y) \geq k$, then still estimate $f(x, y)$ by (7)–(9), after the detected step edge points are replaced by the detected roof/valley edge points in $O_n(x, y)$ when computing the estimator.

4. If $I_n'(x, y) < k$ and $I_n''(x, y) < k$, then estimate $f(x, y)$ by (10) and (11).

In cases when $I_n'(x, y) \geq k$ and $I_n''(x, y) \geq k$, the neighborhood $O_n(x, y)$ likely contains both step and roof/valley edge segments. For instance, on two different sides of a step edge segment in $O_n(x, y)$, the image intensity surface often has different slopes. So, the step edge segment is also a roof/valley edge segment. In such cases, the above BID procedure focuses on the detected step edge points only, because step edges would dominate the roof/valley edges in terms of human visual perception about the image. When we make the judgment whether there are step and/or roof/valley edge segments in $O_n(x, y)$, the number $\gamma_n = k$ is used as a threshold in the above procedure, which is roughly half of the number of pixels on a line that passes (x, y) and is parallel to the x- or y-axis in $O_n(x, y)$. If there is a step (or, roof/valley) edge segment in $O_n(x, y)$ and the threshold value u_n in (6) is properly chosen, then the number of detected step edge points (or, detected roof/valley edge points) should generally be larger than k. Our numerical studies show that other numbers around k (e.g., numbers in $[0.75k, 1.25k]$) can also be

chosen as γ_n; but such choices can hardly improve the estimated image. For this reason, we recommend using $\gamma_n = k$, instead of choosing γ_n separately, to save some computation.

Like most local smoothing estimators, the estimator $\widehat{f}(x,y)$ in (9) or (11) is well defined in $[\xi_n, 1 - \xi_n] \times [\xi_n, 1 - \xi_n]$ only, where $\xi_n = (k + \max(k_1, k_2))/n$. It is not well defined in the border regions of the design space. This is the so-called "boundary problem" in the literature (e.g., Qiu 2005, Section 3.5). There are several existing proposals to overcome this problem. For instance, most DWT software packages use periodic or symmetric "padding" methods to define neighborhoods in the border regions (e.g., Nason and Silverman 1994). In all numerical examples presented in Section 4 of this paper, the symmetric "padding" method is used. By that method, the design space is expanded from $[0, 1] \times [0, 1]$ to $[-\xi_n, 1 + \xi_n] \times [-\xi_n, 1 + \xi_n]$ in the way that the expanded image intensity surface is symmetric about the border of the original design space.

2.3   Selection of procedure parameters

In the proposed BID procedure, there are several parameters to choose. In the image processing practice, people often choose parameter values to be the ones giving the best visual impression. In this part, we provide an alternative approach, which chooses parameters by data-driven procedures.

Our BID procedure consists of two sequential steps for edge detection and for image estimation. Parameters in these two steps can also be chosen sequentially. In the edge detection procedures, there are four parameters k_1, u_n, k_2 and v_n to choose (note: k_2 and v_n are used for roof/valley edge detection). Since detection of step edges is more important to our proposed BID procedure, compared to detection of roof/valley edges, we suggest choosing k_1 and u_n before choosing k_2 and v_n. To this end, we need a performance measure for the set of detected step edges, denoted as $\widehat{S}_n$, in estimating the set of true step edges, denoted as S. In cases when there is no blurring in the observed image Z, Qiu (2002) suggested the following measure:

$$d_Q(\widehat{S}_n, S; k_1, u_n) = w \frac{|\widehat{S}_n \backslash S|}{|\Omega \backslash S|} + (1 - w) \frac{|S \backslash \widehat{S}_n|}{|S|},$$

where $0 \leq w \leq 1$ is a weighting parameter, and $|A|$ denotes the number of design

points in the pointset A. In practice, D can be replaced by $D^* = \{(x_i, y_j) : d_E((x_i, y_j), D) \leq 1/(2n)\}$ for the purpose of calculating d_Q, where d_E is the Euclidean distance. Obviously, $d_Q(\widehat{S}_n, S; k_1, u_n)$ is a weighted average of the proportion of false step edge points detected by (6) and the proportion of true step edge points missed by (6). The weight w represents the relative importance of the first proportion compared to the second proportion, and it should be determined beforehand. In cases when there is no prior information about the relative importance of the proportions, we can simply choose $w = 0.5$.

In simulations, the pointset S is usually known. So, k_1 and u_n can be chosen by minimizing $d_Q(\widehat{S}_n, S; k_1, u_n)$. In practice, however, S is often unknown. In such cases, we propose the following bootstrap procedure. Let

$$\{\widehat{\varepsilon}_{ij} = Z_{ij} - \widehat{a}_0(x_i, y_j), \ \ i, j = 1, 2, \ldots, n\}$$

be the set of residuals obtained from the LLK procedure (10) with the bandwidth k selected separately via the conventional cross validation procedure. Since the mean function of $Z(x, y)$ is $H\{f\}(x, y)$, which is the blurred version of f and which is a continuous function, these residuals should be reasonable estimates of the random errors $\{\varepsilon_{ij}, i, j = 1, 2, \ldots, n\}$ in model (2). Then, we draw n^2 residuals from the above residual set with replacement, and the selected residuals are denoted as $\{\widetilde{\varepsilon}_{ij}^{(1)}, i, j = 1, 2, \ldots, n\}$. The first bootstrap sample is defined by

$$\widetilde{\mathbf{Z}}^{(1)} = \left\{ \widetilde{Z}_{ij}^{(1)} = \widehat{a}_0(x_i, y_j) + \widetilde{\varepsilon}_{ij}^{(1)}, \ \ i, j = 1, 2, \ldots, n \right\}.$$

After repeating this process B times, we get B bootstrap samples $\widetilde{\mathbf{Z}}^{(1)}$, $\widetilde{\mathbf{Z}}^{(2)}$, ..., $\widetilde{\mathbf{Z}}^{(B)}$, where B is the bootstrap sample size. Assume that the detected sets of step edge points from these bootstrap samples are $\widetilde{S}_n^{(1)}, \widetilde{S}_n^{(2)}, \ldots, \widetilde{S}_n^{(B)}$, respectively. Then, k_1 and u_n can be chosen to be the solution of

$$\min_{k_1, u_n} \frac{1}{B} \sum_{l=1}^{B} d_Q \left(\widetilde{S}_n^{(l)}, \widehat{S}_n; k_1, u_n \right). \tag{12}$$

The parameters k_2 and v_n can be chosen similarly. Let RV, $\widehat{RV}_n$, and $\{\widetilde{RV}_n^{(l)}, l = 1, 2, \ldots, B\}$ be the true set of roof/valley edge points, its estimate from the original data, and its estimates from the bootstrap samples, respectively. Then, when RV is known, k_2 and v_n can be chosen by minimizing

13

$d_Q(\widehat{RV}_n, RV; k_2, v_n)$, which is defined similarly to $d_Q(\widehat{S}_n, S; k_1, u_n)$. When RV is unknown, k_2 and v_n can be chosen by minimizing $\frac{1}{B} \sum_{l=1}^{B} d_Q(\widetilde{RV}_n^{(l)}, \widehat{RV}_n; k_2, v_n)$.

After edge detection, we need to choose the bandwidth k used in the BID procedure (8)-(11) for defining the deblurred image $\widehat{f}$. In simulation, the true image f is often known, then k can be selected by minimizing $\text{MSE}(f, \widehat{f}; k) = \frac{1}{n^2} \sum_{i,j=1}^{n} (f(x_i, y_j) - \widehat{f}(x_i, y_j))^2$. In practice, however, f is never known. To this end, cross-validation procedures are natural to consider. But, in the BID model (1), the mean response is the blurred image $H\{f\}(x, y)$, instead of the true image f. So, the cross-validation idea is appropriate only at places where f is continuous because $H\{f\}(x, y)$ and $f(x, y)$ are close if the f is straight around (x, y). On the other hand, observations at those design points that are around edges are affected much by the blur; thus, choosing k by minimizing the distance between individual observations Z_{ij} and the leave-one-out estimates of $f(x_i, y_j)$ may not be appropriate at those places. For this reason, we suggest using the following bootstrap procedure instead. Let $\{\widehat{f}^{(l)}(x, y), l = 1, 2, \ldots, B\}$ be BID estimates of f constructed from the B bootstrap samples $\{\widetilde{\mathbf{Z}}^{(l)}, l = 1, 2, \ldots, B\}$ defined above. Then, k is approximated by the minimizer of

$$\min_k \frac{1}{B} \sum_{l=1}^{B} \left\{ \frac{\widetilde{w}}{|\widehat{S}_n \cup \widehat{RV}_n|} \sum_{(x_i, y_j) \in \widehat{S}_n \cup \widehat{RV}_n} \left[\widehat{f}^{(l)}(x_i, y_j) - \widehat{f}(x_i, y_j) \right]^2 \quad (13)$$

$$+ \frac{(1 - \widetilde{w})}{|\Omega \backslash (\widehat{S}_n \cup \widehat{RV}_n)|} \sum_{(x_i, y_j) \notin \widehat{S}_n \cup \widehat{RV}_n} \left[\widehat{f}^{(l)}_{-(x_i, y_j)}(x_i, y_j) - \widetilde{Z}_{ij}^{(l)} \right]^2 \right\},$$

where $\widehat{f}^{(l)}_{-(x_i, y_j)}(x_i, y_j)$ denotes the leave-one-out estimate at the design point (x_i, y_j) constructed from the bootstrap sample $\widetilde{\mathbf{Z}}^{(l)}$, and $\widetilde{w} \in (0, 1)$ indicates the relative importance of the two quantities. In (13), the first quantity reflects the effectiveness of deblurring around edges while the second one indicates the data fidelity in continuity regions.

When defining $\widehat{f}^{(l)}(x, y)$ from $\widetilde{\mathbf{Z}}^{(l)}$, we suggest using the detected step and roof/valley edge points from the original data (i.e., using $\widehat{S}_n$ and $\widehat{RV}_n$), instead of using detected step and roof/valley edge points from $\widetilde{\mathbf{Z}}^{(l)}$, to save much computation without losing much efficacy. Also, we have used the same bootstrap samples as those used in (12) for simplicity.

14

3   Statistical Properties

We discuss some statistical properties of the proposed edge detection procedures and the BID procedure in this section. In the literature on image deblurring, the psf $h(u, v; x, y)$ in model (1) is usually assumed to be a density function since it is believed that the blurring process would not change the image mass (cf., Bates and McDonnell 1986). This conventional assumption is also adopted here. Furthermore, we assume that $h(u, v; x, y) = 0$ if $\sqrt{u^2 + v^2} > r_n(x, y)/n$, where $r_n(x, y)$ is a positive integer indicating the number of rows/columns of pixels that are affected by the blur at (x, y). Theorem 3.1 below gives some results about the detected step and roof/valley edge points. In the theorem, the following notations are used: $\Omega_{k_1,n} = \{(x_i, y_j) : (x_i, y_j) \in [k_1/n, 1 - k_1/n] \times [k_1/n, 1 - k_1/n]\}$, J_S includes all singular points in S, defined to be crossing points of step edge segments, points on a single step edge segment at which there does not exist a unique tangent line of the edge segment, or points on a single step edge segment at which the jump sizes in f are 0, $J_{S,k_1,n} = \{(x, y) : d_E((x, y), (x', y')) \le k_1/n, \text{ for any } (x', y') \in J_S\}$, $\overline{J}_{S,k_1,n} = \Omega \backslash J_{k_1,n}$, $S_{k_2,n} = \{(x, y) : d_E((x, y), (x', y')) \le k_2/n, \text{ for any } (x', y') \in S\}$, $\overline{S}_{k_2,n} = \Omega \backslash S_{k_2,n}$, $\Omega_{k_2,n}$ is defined similarly to $\Omega_{k_1,n}$, J_{RV} includes all singular points on RV defined similarly to J_S, $\overline{J}_{RV,k_2,n}$ is defined similarly to $\overline{J}_{S,k_1,n}$, and

$$d_H(A, B) = \max \left\{ \sup_{\mathbf{s_1} \in A} \inf_{\mathbf{s_2} \in B} d_E(\mathbf{s_1}, \mathbf{s_2}), \ \sup_{\mathbf{s_1} \in B} \inf_{\mathbf{s_2} \in A} d_E(\mathbf{s_1}, \mathbf{s_2}) \right\}$$

is the Hausdorff distance between two pointsets A and B.

Theorem 3.1. *Assume that the true image intensity function f has piecewisely continuous second-order derivatives in each closed subset of $[0, 1] \times [0, 1]$ where f and its first-order derivatives are continuous; at the boundary curves of the pieces, f has uniformly bounded, directional second-order derivatives from any direction in a single piece; f also has uniformly bounded, directional first-order derivatives at any point in RV from any direction passing through a region that the first-order derivatives are continuous; $E(\varepsilon_{11}^3) < \infty$; the kernel function K^* is a Lipschitz-1 continuous, circularly symmetric, density function; the kernel function L^* is a Lipschitz-1 continuous increasing density function supported on $[0, 1]$; the psf $h(u, v; x, y)$ is bounded uniformly with respect to (u, v) and (x, y); the blurring extent $R_n = \sup_{i,j} r_n(x_i, y_j)$, the bandwidths k_1, k_2, and the sample size n satisfy the conditions that $k_1/n = o(1)$, $k_2/n = o(1)$, $1/k_1 = o(1)$, $1/k_2 = o(1)$, $R_n/k_1 = o(1)$, $R_n/k_2 = o(1)$, $n^2 \log(n)/k_1^3 = O(1)$ and $n^2 \log(n)/k_2^3 = O(1)$; u_n*

and v_n satisfy the conditions that $k_1^2/(nu_n) = o(1)$, $u_n/k_1 = o(1)$, $k_1^2/(nv_n) = o(1)$, and $v_n/k_1 = o(1)$. Then, we have

(i) $d_H\left(\widehat{S}_n \bigcap(\Omega_{k_1,n} \bigcap \overline{J}_{S,k_1,n}), \; S\bigcap(\Omega_{k_1,n} \bigcap \overline{J}_{S,k_1,n})\right) = O(k_1/n), \; a.s., \; and$

(ii) $d_H\left(\widehat{RV}_n \bigcap(\Omega_{k_2,n} \bigcap \overline{S}_{k_2,n} \bigcap \overline{J}_{RV,k_2,n}), \; RV\bigcap(\Omega_{k_2,n} \bigcap \overline{S}_{k_2,n} \bigcap \overline{J}_{RV,k_2,n})\right)$
$\quad = O(k_2/n), \; a.s..$

Remark 3.1 By Theorem 3.1, the detected step edge pointset $\widehat{S}_n$ converges almost surely to the true step edge pointset S in Hausdorff distance, after some small regions around the singular points of S and the border of the design space are excluded. Regarding the detected roof/valley edge pointset $\widehat{RV}_n$, Theorem 3.1 says that it converges almost surely to the true roof/valley edge pointset RV in Hausdorff distance, after some small regions around the step edge pointset S, the singular points of RV and the border of the design space are excluded.

Remark 3.2 In Theorem 3.1, it is assumed that $R_n/k_1 = o(1)$. By this assumption, the number of rows/columns of pixels affected by blur (i.e., R_n) is allowed to tend to infinity, but the rate needs to be slower than that of the number of pixels used in local smoothing (i.e., k_1). In terms of the image acquisition, this assumption implies that when the image acquisition techniques are improved so that the image resolution is increased (i.e., n is increased), R_n can increase with n. But, to have a good blind image deblurring result using our method, R_n cannot increase too fast. Intuitively, this requirement seems reasonable because when image acquisition techniques are improved, the number of rows/columns of pixels affected by blur should be under control.

The next theorem establishes the statistical consistency of the deblurred image by the proposed BID procedure (8)–(11). Proofs of the two theorems are given in the Supplementary file.

Theorem 3.2. *Under the conditions stated in Theorem 3.1, if we further assume that $k_1/k = o(1)$ and $k_2/k = o(1)$, then we have*

(i) for any given point $(x,y) \in \Omega_{k,n}\backslash(S\bigcup RV)$,

$$\widehat{f}(x,y) = f(x,y) + O(k/n) + O\left(\frac{\log(n)}{k}\right), \; a.s.,$$

(ii) for any given point $(x, y) \in \Omega_{k,n} \bigcap (S \setminus J_S)$,

$$\widehat{f}(x,y) = f(x,y) - C(x,y)C_{K,L} + O(k/n) + O(k_1/k) + O\left(\frac{\log(n)}{k}\right), \; a.s.,$$

where $C(x, y)$ is the jump magnitude of f at (x, y),

$$C_{K,L} = \frac{\int_0^1 \int_{-1}^1 K(s,t)dt L(s) \int_{u>s\frac{k}{r_n(x,y)}} \widetilde{h}(u,v;x,y)dudvds}{\int_0^1 \int_{-1}^1 K(s,t)dt \; L(s)ds},$$

$\widetilde{h}(u,v;x,y) = h(u\cos\theta + v\sin\theta, -u\sin\theta + v\cos\theta; x, y)$, and θ is the acute angle formed by the tangent line of S at (x, y) and the y-axis.

(iii) for any given point $(x, y) \in \Omega_{k,n} \bigcap (RV \setminus J_{RV})$,

$$\widehat{f}(x,y) = f(x,y) + O(k/n) + O(k_2/k) + O\left(\frac{\log(n)}{k}\right), \; a.s.,$$

where $\Omega_{k,n}$ is defined similarly to $\Omega_{k_1,n}$ used in Theorem 3.1.

Remark 3.4 Result (i) in Theorem 3.2 establishes the consistency for $\widehat{f}(x,y)$ in continuity regions of f. Result (ii) is about the property of $\widehat{f}(x,y)$ around step edges. It can be checked that the second term on the right hand side of the equation for $\widehat{f}(x,y)$ is of order $O(R_n/k)$. So, under the conditions stated in the theorem, $\widehat{f}(x,y)$ is a consistent estimator of $f(x,y)$ around step edges. Furthermore, if the kernel function L is increasing on $[0,1]$, then by the Chebyshev integral inequality (cf., Mitrinovic, Pecaric and Fink 1993), we have

$$C_{K,L} \leq \frac{\int_0^1 \int_{-1}^1 K(s,t) \; dt \; \int_{u>s\frac{k}{r_n(x,y)}} \widetilde{h}(u,v;x,y) \; dudv \; ds}{\int_0^1 \int_{-1}^1 K(s,t) \; dt \; ds}.$$

The right-hand-side of the above inequality is the leading term of the asymptotic bias caused by blur of $\widehat{f}(x,y)$ for estimating $f(x,y)$ in cases when L is not used in constructing $\widehat{f}(x,y)$. This result shows that L used in (8) is helpful in reducing the asymptotic bias of $\widehat{f}(x,y)$. Result (iii) in the theorem is about the property of $\widehat{f}(x,y)$ around roof/valley edges. The asymptotic bias of $\widehat{f}(x,y)$ in this case can be studied in a similar way to that in result (ii). It is omitted here.

4 Numerical Studies

In this section, we present some numerical examples concerning the numerical performance of the proposed BID procedure (8)–(11). Throughout this section,

if there is no further specification, the kernel functions K^* and K are both chosen to be the truncated Gaussian density functions, i.e., $1/(2\pi - 3\pi \exp(-0.5))$ $[\exp(-(x^2 + y^2)/2) - \exp(-0.5)]I_{x^2+y^2 \leq 1}$, the kernel functions L^* and L are both chosen to be $1/1.194958 \exp(x^2/2)I_{0 \leq x \leq 1}$, which is proportional to the reciprocal of the 1-D truncated Gaussian density function, w in (12) and $\widetilde{w}$ in (13) are both fixed at 0.5, and B in (12) and (13) is chosen to be 100. Degraded images are generated from model (2), in which the psf is chosen to be

$$h(u, v; x, y) = \frac{3}{\pi} \left(1 - \frac{\sqrt{u^2 + v^2}}{r_n(x, y)/n} \right) I_{\sqrt{u^2+v^2} \leq r_n(x,y)/n},$$

and the additive random errors ε_{ij} follow the distribution $N(0, \sigma^2)$. The above psf is circularly symmetric with the blurring extent $r_n(x, y)$ which may depend on (x, y). Let $\rho_n(x, y) = r_n(x, y)/n$ denote the blurring-extent-to-sample-size ratio (BSR) at (x, y). Two artificial numerical examples are presented in the supplementary file, from which we can see that our proposed BID procedure (8)–(11) performs well in various cases. Next, we consider the test image of peppers with 256×256 pixels shown in Figure 3, and compare our proposed BID procedure with three representatives of the existing deblurring methods. The first existing method considered here is the one accomplished by the Matlab's blind deconvolution routine *deconvblind*, which is based on the method discussed by Biggs and Andrews (1997) and Jansson (1997) in the framework of the Richardson-Lucy algorithm. The second method is the total-variation-based image deblurring method proposed by Oliveira, Bioucas-Dias, and Figueiredo (2009). The third method is the blind image deconvolution procedure developed under the Bayesian framework by Fergus, Singh, Hertzmann, Roweis and Freeman (2006). These methods are denoted as RL, TV and Bayes, respectively. It should be pointed out that both RL and Bayes are blind image deblurring schemes, but TV requires the psf h to be fully specified.

The example is set up as follows. The original test image is first blurred by the psf h with three different BSR functions: $\widetilde{\rho}_n^{(1)}(x, y) = 0.03(1 - (x - 0.5)^2 - (y - 0.5)^2)$, $\widetilde{\rho}_n^{(2)}(x, y) = 0.03x$, and $\widetilde{\rho}_n^{(3)}(x, y) = 0.02$. Then, additive random noise generated from the $N(0, \sigma^2)$ distribution is added to the blurred test image, where σ is fixed at 5 or 10. Figure 4(a) presents the degraded test image in the case with $\widetilde{\rho}_n^{(2)}$ and $\sigma = 10$. The deblurred image by our BID method with the bandwidth

18

Figure 3: Original test image of peppers.

k/n chosen to be $5/256$ is shown in Figure 4(b). The deblurred image by RL is shown in Figure 4(c). Note that the RL algorithm is designed to handle location-invariant blur only, and the blurring extent r_n needs to be specified beforehand. In our simulation, r_n is selected by minimizing the mean squared error of the deblurred image so that it can have its best performance in the example. The TV procedure requires the specification of h beforehand. In this example, we have tried two different ways for that purpose. One is that the true expression of h is used, and the second way is that h is assumed to be the psf of a motion blur along the x-axis (i.e., $h(u,v;x,y) = \frac{2n}{r_n}I_{\{|u|\leq r_n/n\}}\delta_0(v)$, where δ_0 is a point mass at 0). The two different versions of the TV procedure are denoted as TV1 and TV2 hereafter, and their deblurred images are shown in Figure 4(d) -(e). To implement the Bayes method, a sub-region of the image needs to be chosen beforehand. As suggested in Fergus, Singh, Hertzmann, Roweis, and Freeman (2006), their algorithm would perform better and run faster if a smaller patch, rich in edge structure, is manually selected. Based on our visual impression of the test image, we choose the sub-region $[25/256, 75/256] \times [25/256, 75/256]$, and the deblurred image is shown in Figure 4(f). From the figure, it can be seen that (i) our proposed method can remove both noise and blur reasonably well, (ii) the deblurred image by RL contains much noise and some artifacts, (iii) the TV1 method, in which the form of the psf h is correctly specified, cannot handle spatially-variant blur well, in that much artifacts are generated at the boundaries

of the image while its deblurred image in the central part looks reasonably good, (iv) the TV2 method, in which a wrong psf is specified, performs poorly, and (v) the Bayes method performs poorly as well due to the facts that the observed test image contains much noise and that the method is developed mainly for handling motion blur which is not the case in the current example. We have tried several different choices of the sub-region when implementing the Bayes method. No significant improvement in the results can be obtained.
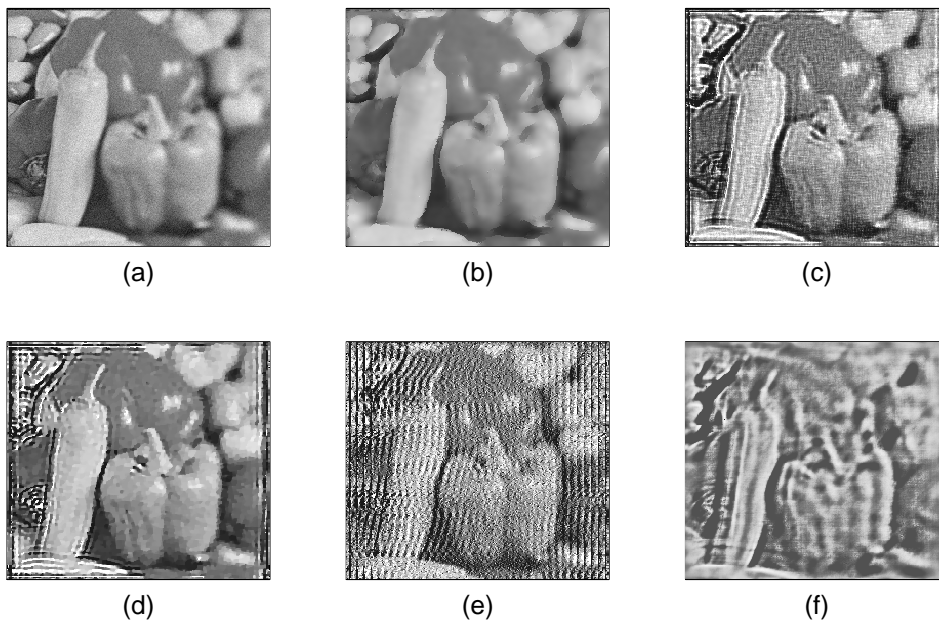

(a) (b) (c)

(d) (e) (f)

Figure 4: (a): Observed test image of peppers in the case when $\rho_n(x, y) = 0.03x$ and $\sigma = 10$. (b)-(f): Deblurred images by NEW, TV when h is specified correctly, TV when h is specified incorrectly, and Bayes, respectively.

Figure 5 presents the corresponding results in cases when $\widetilde{\rho}_n^{(3)}(x, y) = 0.02$ and $\sigma = 10$. In such cases, the spatial blur is location invariant. From the figure, it can be seen that (i) our proposed method sharpens the observed test image much, (ii) the deblurred image by RL contains much noise and many artifacts as before, (iii) the TV method performs well when the true psf h is fully specified, (iv) the TV method does not perform well when h is misspecified, and (v) the Bayes method performs poorly once again.

Table 1 presents the root mean squared errors (RMSE) of the four deblur-
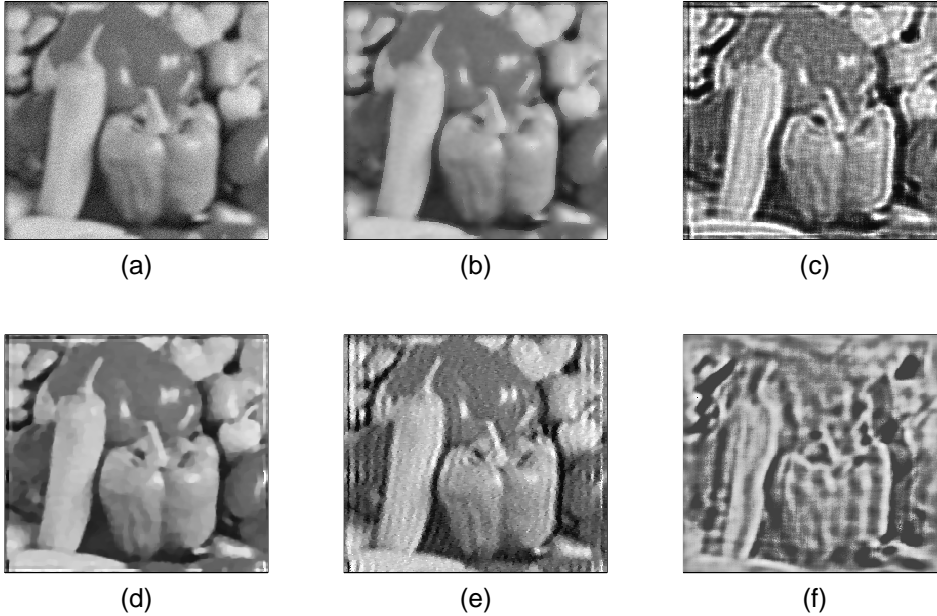
Figure 5: (a): Observed test image of peppers in the case when $\rho_n(x, y) = 0.02$ and $\sigma = 10$. (b)-(f): Deblurred images by NEW, TV when h is specified correctly, TV when h is specified incorrectly, and Bayes, respectively.

ring methods, based on 100 replicated simulations. In the table, the proposed BID method is denoted as NEW. It can be seen that (i) the proposed method outperforms the other methods in most cases considered, and it can handle a wide variety of blurs since it does not require any restrictive conditions on the psf h, (ii) the TV method performs the best in cases when the true psf is location-invariant and fully specified (i.e., the case when $\rho_n(x, y) = \widetilde{\rho}_n^{(3)}(x, y)$ for TV1), (iii) the TV method could perform poorly when h is misspecified (i.e., TV2), and (iv) both the RL and Bayes methods cannot deblur the image well.

5 Discussions

We have described our proposed method for blind image deblurring in the previous sections. Our method differs from most existing methods by imposing little restriction on the psf h and the true image intensity function. It even allows the psf h to be spatially variant. Our method makes use of the hierarchical structure

Table 1: RMSE values of the four image deblurring methods in the example of the test image of peppers.

Methods	$\widetilde{\rho}_n^{(1)}(x,y)$		$\widetilde{\rho}_n^{(2)}(x,y)$		$\widetilde{\rho}_n^{(3)}(x,y)$	
	$\sigma = 5$	10	$\sigma = 5$	10	$\sigma = 5$	10
NEW	19.18	19.37	18.14	19.34	18.07	18.40
RL	30.32	33.66	49.18	52.58	37.90	40.14
TV1	19.40	19.64	64.79	64.59	17.66	17.75
TV2	27.71	36.84	76.27	103.29	20.73	29.36
Bayes	33.78	45.06	42.44	52.81	46.48	48.99

of blurred images by paying special attention to regions around the detected step and valley/roof edges. Also, a data-driven parameter selection scheme based on bootstrap has been suggested. Both theoretical justifications and numerical studies show that our method can remove pointwise noise and spatial blur well in various cases.

The proposed method still has much room for further improvements. For instance, the current version of the method uses constant bandwidth and threshold parameters in step edge and roof/valley edge detection and in image deblurring as well. The idea of multilevel smoothing with location-variant bandwidths and threshold values can be incorporated into the proposed method. In such cases, one price to pay is the expensive computation. Furthermore, our current method cannot provide an estimate for the psf h. It requires much future research to modify it properly such that h can be estimated accurately at the same time when the observed image is deblurred.

References

Bates, R.H.T. and McDonnell, M.J. (1986). *Image Restoration and Reconstruction.* Oxford: Clarendon Press.

Biggs, D. and Andrews, M. (1997) . Acceleration of iterative image restoration algorithms. *Applied Optics.* **36, 8**, 1766–1775.

Canny, J. (1986). A computational approach to edge detection. *IEEE Transactions on Pattern Analysis and Machine Intelligence.* **8**, 679–698.

Carasso, A.S. (2001). Direct blind deconvolution. *SIAM Journal on Applied Mathematics.* **61**, 1980–2007.

Chan, T.F. and Wong, C.K. (1998). Total variation blind deconvolution. *IEEE Transactions on Image Processing.* **7**, 370–375.

Chu, C.K., Siao, J.S., Wang, L.C., and Deng, W.S. (2012). Estimation of 2D jump location curve and 3D jump location surface in nonparametric regression. *Statistics and Computing.* **22**, 17–31.

Fergus, R., Singh, B., Hertzmann, A., Roweis, S. T., and Freeman, W.T. (2006). Removing Camera Shake From A Single Photograph. *ACM Transactions on Graphics.* **25**, 787–794.

Figueiredo, M.A.T. and Nowak, R.D. (2003). An EM algorithm for wavelet-based image restoration. *IEEE Transactions on Image Processing.* **12**, 906–916.

Garlipp, T. and Müller, Ch.H. (2007). Robust jump detection in regression surface. *Sankhya (Series B).* **69**, 55–86.

Gonzalez, R.C. and Woods, R.E. (1992). *Digital Image Processing.* Addison-Wesley Publishing Company, Inc.

Hall, P. and Qiu, P. (2007a). Blind deconvolution and deblurring in image analysis. *Statistica Sinica.* **17**, 1483–1509.

Hall, P. and Qiu, P. (2007b). Nonparametric estimation of a point spread function in multivariate problems. *The Annals of Statistics*, **35**, 1512–1534.

Jansson, P. A. (1997). *Deconvolution of Images and Spectra*, Academic Press.

Joshi, M.V. and Chaudhuri, S. (2005). Joint blind restoration and surface recovery in photometric stereo. *Journal of the Optical Society of America, Series A.* **22**, 1066–1076.

Katsaggelos, A.K. and Lay, K.-T. (1990). Image identification and image restoration based on the expectation-maximization algorithm. *Optical Engineering.* **29**, 436–445.

Kundur, D. and Hatzinakos, D. (1996). Blind image deconvolution. *IEEE Signal Processing Magazine.* **13**, 43–64.

Kundur, D. and Hatzinakos, D. (1998). A novel blind deconvolution scheme for image restoration using recursive filtering. *IEEE Transactions on Signal Processing.* **46**, 375–390.

Levin, A., Weiss, Y., Durand, F., and Freeman, W.T. (2011). Understanding blind deconvolution algorithms. *IEEE Transactions on Pattern Analysis and Machine Intelligence.* **33**, 2354–2367.

Likas, A.C. and Galatsanos, N.P. (2004). A variational approach for Bayesian blind image deconvolution. *IEEE Transactions on Signal Processing.* **52**, 2222–2233.

Miskin, J. and MacKay, D.J.C. (2000). Ensemble Learning for Blind Image Separation and Deconvolution. *Proc. Advances in Independent Component Analysis.* M. Girolani, Ed. Springer-Verlag.

Mitrinovic, D., Pecaric, J., and Fink, A. (1993). *Classical and New Inequalities in Analysis*, Kluwer Academic Publishers.

Nason, G., and Silverman, B. (1994). The discrete wavelet transform in S. *Journal of Computational and Graphical Statistics.* **3**, 163–191.

Oliveira, J.P., Bioucas-Dias, J., and Figueiredo, M. (2009). Adaptive total variation image deblurring: A majorization-minimization approach. *Signal Processing*, **89**, 1683-1693.

Pruessner, A., and O'Leary, D.P. (2003). Blind deconvolution using a regularized structured total least norm algorithm. *SIAM Journal on Matrix Analysis and Applications*, **24**, 1018-1037.

Qiu, P. (1998). Discontinuous regression surfaces fitting. *The Annals of Statistics.* **26**, 2218–2245.

Qiu, P. (2002). A nonparametric procedure to detect jumps in regression surfaces. *Journal of Computational and Graphical Statistics.* **11**, 799–822.

Qiu, P. (2005). *Image Processing and Jump Regression Analysis.* New York: John Wiley & Sons.

Qiu, P. (2008). A nonparametric procedure for blind image deblurring. *Computational Statistics and Data Analysis.* **52**, 4828–4841.

Qiu, P. (2009). Jump-preserving surface reconstruction from noisy data. *Annals of the Institute of Statistical Mathematics.* **61**, 715–751.

Qiu, P. and Yandell, B. (1997). Jump detection in regression surfaces. *Journal of Computational and Graphical Statistics.* **6**, 332–354.

Rudin, L.I., Osher, S., and Fatemi, E. (1992). Nonlinear total variation based noise removal algorithms *Physica D.* **60**, 259–268.

Skilling, J. (1989, eds). *Maximum Entropy and Bayesian Methods.* Norwell, MA: Kluwer Academic.

Sun, J. and Qiu, P. (2007). Jump detection in regression surfaces using both first-order and second-order derivatives. *Journal of Computational and Graphical Statistics.* **16**, 289–311.

Yang, Y., Galatsanos, N.P., and Stark, H. (1994). Projection-based blind deconvolution. *Journal of the Optical Society of America A.* **11**, 2401–2409.

You, Y.L. and Kaveh, M. (1996). A regularization approach to joint blur identification and image restoration. *IEEE Transactions on Image Processing.* **5**, 416–428.

Department of Biostatistics, University of Florida

E-mail: pqiu@ufl.edu

Department of Biostatistics, University of Florida

E-mail: kangx276@ufl.edu